Flow-enhanced magnetic resonance imaging

Thomas L. Chenevert
Department of Radiology, University of Michigan Medical Center, Ann Arbor, Michigan 48109

(Received 6 May 1985; accepted for publication 7 November 1985)

A new technique for detecting blood flow in magnetic resonance imaging is proposed. This technique is tailored to enhance areas containing flow while suppressing static and nonsignal areas with the objective of optimizing the contrast of vascularized tumors. Unlike flow phase imaging, in-plane flow directionality (parallel versus antiparallel to applied flow gradient) is removed by the proposed method to reduce phase cancellation of flow signals. This signal loss is apt to occur in instances of complicated vascularity patterns consisting of many small vessels having multiple flow directions. The new flow-enhanced imaging method is compared to flow phase imaging by computer simulation of simple objects containing many small vessels. The results indicate that flow-enhanced imaging yields significantly greater detectability of regions of complicated small-vessel patterns than phase imaging.

INTRODUCTION

A variety of magnetic resonance imaging (MRI) techniques have been introduced designed to measure dynamic processes of blood flow. These methods exploit effects on either the amplitude or phase of spins flowing through the imaging plane, which alter measured magnetization. Amplitude-dependent measures of flow generally monitor blood flow perpendicular to the imaging plane and are sometimes referred to as time-of-flight techniques.[1] Selective excitation of spins within a plane in conjunction with selective refocusing in a plane various distances downstream yield signals exclusively from spins flowing plane-to-plane.[2] Alternatively, one can monitor the rate of replenishment of magnetization from protons flowing into the imaging plane which have not experienced the previous saturating 90° rf pulse.[3,4]

The phase of spins traversing a magnetic field gradient is also altered relative to static spins. Flow phase effects have been observed in multiecho spin-echo sequences, where even-numbered spin echoes yield an unusually strong signal compared to odd-numbered echoes.[5] The phase accrued due to a spin traversing a field gradient applied during odd echoes is cancelled by the phase accumulated during generation of the subsequent echo. Therefore, regardless of their flow speed, spins are refocused into a coherent strong signal on even echoes.

Flow-related phase effects may be studied more directly by production of phase images, whereby the phase angle of each complex valued pixel is displayed. Under ideal conditions in which a motionless object is imaged by a perfect machine having no miscellaneous systematic phase errors, the reconstructed image is purely real valued (phase = 0). For the purpose of conventional imaging, real systems mitigate systematic phase errors by retention of only the modulus of each reconstructed pixel value. Since flow is a nonsystematic contributor to phase shifts, it can be studied via phase images in which systematic phase shifts are subtracted or are negligible.[6,7] Application of conventional imaging gradients inherently produce phase shifts in the presence of flow[8,9]; however, several alternative flow measurement techniques rely on special flow-sensitizing gradients.[10–12]

An alternative method for flow detection, termed "flow-enhanced MRI," is presented below, where the objective is to increase detectability of flow in an entanglement of small vessels which has flow in many directions. Phase display and time-of-flight methods are not well suited to flow detection in such instances. The flow-enhanced method proposed here does not attempt to quantify magnitude nor direction of flow, but rather generate an image in which areas of flowing blood are enhanced and static tissues are suppressed to a level equivalent to that of nonsignal areas. This is in contrast to phase images in which nonsignal areas appear as noise, having the full range of image brightness values ($\pm\pi$), signal-producing static tissues appear as midgray (phase = 0), and forward and reverse flow directions relative to the flow-encoding gradient appear as brighter and darker areas, respectively. Since forward and reverse flow are distinguished in phase images, it is possible that their effects may partially or completely cancel when both are present within a single voxel. The flow-enhanced method is designed to treat forward and reverse flow equivalently, thereby removing these phase cancellation effects. These distinctions from phase imaging are anticipated to offer greater sensitivity to highly vascularized tumors containing many small, intertwined vessels such as those in breast tumors. Often these tumor vessels exhibit unusually high flow velocities for their size.[13]

THEORY

In conventional nuclear magnetic resonance (NMR) imaging, field gradients are applied along three spatial directions to excite and encode planes of precessing transverse magnetization. It has been shown that in the presence of imaging field gradients $\mathbf{g}$, signals S induced in the receiver coil by the transverse magnetization are related to the distribution of transverse magnetization M by the two-dimensional Fourier transform,

$$S(\mathbf{g}) = \int M(\mathbf{r}) e^{i2\pi\gamma \mathbf{g}\cdot\mathbf{r}} d^2r, \quad (1)$$

 0094-2405/86/020177-05$01.20

where γ is the gyromagnetic ratio of protons. In Eq. (1) and in the following discussion, it is assumed that signals are demodulated by a quadrature receiver producing two output signals (the real and imaginary components of S) such that magnetization is measured in a frame rotating at the Larmor frequency of protons in the static field. Also, only a two-dimensional transform is used since it is assumed that single planes through the object are excited individually.

In addition to encoding the spatial distribution of M, gradients may be employed to encode the distribution of flow speeds within the objects. Moran[10] outlined a scheme to generate the full six-dimensional space of $M(\mathbf{r},\mathbf{v})$ using bipolar gradients. This task would be too time consuming for many applications; therefore simplifications have been proposed, such as phase imaging, where an imaging gradient or additional flow-sensitizing gradient induces the desired flow phase shift. The phase change due to motion $\varphi(\mathbf{v})$ of a precessing spin initially at position $\mathbf{r}$, traveling with speed $\mathbf{v}$ after experiencing a bipolar gradient $\mathbf{F}(t)$, is given by

$$\begin{aligned}\varphi(\mathbf{v}) &= 2\pi\gamma \int_0^{2t_0} \mathbf{F}(t)\cdot(\mathbf{r}+\mathbf{v}t)\,dt \\ &= 2\pi\gamma\mathbf{F}_0\cdot\mathbf{v}t_0^2, \end{aligned} \tag{2}$$

where

$$\mathbf{F}(t) = \begin{cases} +\mathbf{F}_0 & 0<t\leqslant t_0 \\ -\mathbf{F}_0 & t_0<t\leqslant 2t_0 \\ 0 & |t-t_0|>t_0 \end{cases}. \tag{3}$$

Notice that the antisymmetric $\mathbf{F}(t)$ gradient induces phase shifts proportional to flow speed without affecting spatial encoding, since the result is independent of $\mathbf{r}$. Consequently, a display of the reconstructed image phase would have gray scale values proportional to flow velocity along the direction parallel to $\mathbf{F}_0$. Knowledge of the maximum expected flow speed allows one to choose $F_0t_0^2$ such that the greatest phase shift is slightly less than π. This affords maximum sensitivity to flow phase shifts without having forward flow aliased into negative flow phase shifts and vice versa. Several groups have reported successful results using this or closely related approaches when measuring flow in large tubes or vessels.

Notice that the above method will experience phase cancellations and reduced sensitivity to flow when several small vessels intersect a single voxel having components of flow in multiple opposing directions. It is anticipated that this situation is a common occurrence in highly vascularized tumors for which the following flow detection sequence is proposed.

Let $S(\mathbf{g}, 0)$ denote the complex data set acquired with only conventional imaging gradients, with $S(\mathbf{g}, +\mathbf{F}_0)$ as the data set acquired with an additional flow gradient given by Eq. (3), and $S(\mathbf{g}, -\mathbf{F}_0)$ as the data set acquired with a flow gradient having opposite polarity of that of Eq. (3). Consider the following weighted sum of their three data sets:

$$S(\mathbf{g}) = S(\mathbf{g},0) - \tfrac{1}{2}[S(\mathbf{g}, +\mathbf{F}_0) + S(\mathbf{g}, -\mathbf{F}_0)], \tag{4}$$

where

$$S(\mathbf{g}, \pm\mathbf{F}_0) = \int M(\mathbf{r},\mathbf{v}) e^{i2\pi\gamma\mathbf{g}\cdot\mathbf{r}} e^{\pm i2\pi\gamma\mathbf{F}_0\cdot\mathbf{v}t_0^2}\, d^2r\, dv.$$

While the flow velocity integration is over all three directions, only flow velocities having a component colinear with the direction designated by the flow gradient become phase shifted. The results of the sum will be

$$S(\mathbf{g}) = \int M(\mathbf{r},\mathbf{v}) e^{i2\pi\gamma\mathbf{g}\cdot\mathbf{r}} [2\sin^2(\pi\gamma\mathbf{F}_0\cdot\mathbf{v}t_0^2)]\, d^2r\, dv, \tag{5}$$

which is available for two-dimensional digital Fourier transform (2D-DFT) reconstruction to yield $S(r)$, from which a flow-enhanced image is derived,

$$\begin{aligned} S(\mathbf{r}) &= \int M(\mathbf{r},\mathbf{v})[2\sin^2(\pi\gamma\mathbf{F}_0\cdot\mathbf{v}t_0^2)]\, dv, \\ I(\mathbf{r}) &= |S(\mathbf{r})|. \end{aligned} \tag{6}$$

Equation (4) indicates that data sets are combined prior to reconstruction; however, the operations of reconstruction and summation are interchangeable as long as the complex nature of the data is maintained. As with conventional images, miscellaneous systematic phase errors are removed by taking the modulus of $S(\mathbf{r})$ as the image. Such an image would display static tissue [weighted by $\sin(0)=0$] and nonsignal producing areas (weighted by $M=0$) as low intensity, while enhancing regions containing flow. Furthermore, opposing flow directions are weighted equivalently in the integrand of Eq. (6), thereby obviating flow phase cancellation within individual voxels. This precaution against flow signal loss to phase cancellation comes at the expense of acquisition time, since three data sets are required. To reduce scan time, an approximation to Eq. (6) is realized by simply subtracting data acquired with a flow gradient applied from non-flow-encoded data. Rather than $2\sin^2(\pi\gamma\mathbf{F}_0\cdot\mathbf{v}t_0^2)$, the weighting of $M(\mathbf{r},\mathbf{v})$ would be

$$2\sin^2(\pi\gamma\mathbf{F}_0\cdot\mathbf{v}t_0^2) - i\sin(2\pi\gamma\mathbf{F}_0\cdot\mathbf{v}t_0^2).$$

The second term, being an odd function in $\mathbf{v}$, will cancel forward with reverse flow; however, the first term insures against a complete negation of flow signals. It is not recommended that only the real component of the reconstructed pixel values be retained in order to eliminate this odd function weighting, since systematic phase errors would then become a factor.

In the following computer simulations, flow-enhanced images are compared to phase images where a single flow-encoding gradient is applied. The reconstructed result $S(\mathbf{r})$, and the corresponding values $I(\mathbf{r})$ ultimately displayed in the phase image are

$$\begin{aligned} S(\mathbf{r}) &= \int M(\mathbf{r},\mathbf{v}) e^{i2\pi\gamma\mathbf{F}_0\cdot\mathbf{v}t_0^2}\, dv, \\ I(\mathbf{r}) &= \tan^{-1}\left\{\frac{\mathrm{Im}[S(\mathbf{r})]}{\mathrm{Re}[S(\mathbf{r})]}\right\}. \end{aligned} \tag{7}$$

Inspection of Eq. (7) indicates that forward flow phase shifts are countered by reverse flow such that, in extreme cases, little or no flow phase shifts may be registered in the presence of high flow.

COMPUTER SIMULATIONS

Equations (6) and (7) were used as a basis of computer simulations to compare the performance of phase imaging of flow and flow-enhanced imaging. The simulated object was prescribed to have three types of regions, diagramed in Fig. 1: nonsignal, high-signal static tissue, and high-signal static tissue including vessels of flowing blood. Since Eqs. (6) and (7) were used, it is emphasized that the images were synthesized pixel by pixel in the spatial domain and not as spin echoes followed by 2D-DFT reconstruction, as would be implemented on an actual system. This implies that several assumptions were employed. First, in the vessel there is continuous nonpulsatile plug flow throughout the data acquisition period. The assumption of plug flow is not significant since we are not attempting to quantify flow volume. Pulsatile flow would result in variable flow phase shifts at the time of each spatial phase-encoding gradient application. As in conventional phase-encoding imaging, this additional pseudorandom phase would manifest itself within the image as a band of noise in which the vessel's location is scattered along the phase-encoding gradient direction. However, cardiac gating is a means to acquire data under approximately continuous flow conditions.

Another assumption is that only the flow-encoding gradient alters the phase of the flowing spins (i.e., flow phase shifts are unaffected by the spatial encoding gradients). This is not true if conventional imaging gradients are applied; however, special imaging gradient protocols are available which uncouple **g** and **v**, as implied in Eq. (4). A tripolar gradient: positive for duration τ, negative for duration 2τ, then positive again such that the spin-echo peak occurs a time τ after switching positive, provides spatial frequency encoding while greatly reducing flow phase shifts. In essence, this spatial encoding gradient rephases signals from moving protons, regardless of their flow speed, in a manner similar to even-echo rephasing[5]; however, this occurs on an odd (first) echo. In addition to uncoupling **g** and **v**, as desired, imaging gradients of this type should be valuable in conventional imaging in reducing motion-related phase errors, which appear as ghosts and bands of increased noise along the phase-encoding direction of the image.

Finally, it is assumed that there are no spatially dependent systematic phase errors. While these phase errors have no impact on the flow-enhanced image, since only the modulus is retained, they would affect the phase images. Consequently, practical application of the phase image approach would require these errors to be minimal, or at least subtractable from the image. Therefore, while these assumptions imply nearly ideal conditions, it is the goal of this work to compare the two methods under equivalent conditions to gauge their relative merit in detection of small-vessel flow.

The simulation algorithm generated N straight vessels of equal width w, all having equal constant flow of speed v. The (x, y) coordinates of a point intersected by each vessel P, along with flow direction θ, were selected by a random number generator. A flow-encoding gradient along the x direction (horizontal) was simulated such that $2\pi\gamma F_0 t_0^2 = 0.6$ rad/cm/s. For each pixel within the central square containing the vessels, a sum was performed over all N vessels of the phase-shifted signal [Eq. (2)] weighted by the intersection area of the pixel and the vessel. After this summation, the residual area of each pixel (i.e., the difference between pixel area and net area of vessel intersection) was defined as the non-phase-shifted signal. Intersection areas were used as weighting coefficients of flow and nonflow components of signal from each pixel since the simulation is two-dimensional in nature. In reality, weighting would be determined by the intersection volume of the vessel with each voxel. For example, a 0.2-mm-wide vessel traversing a 2×2 mm pixel in simulation corresponds to a 1.6-mm caliber vessel if the imaged plane in reality has a 10-mm thickness.

The amplitudes of each pixel in the signal areas (with and without vessels) and nonsignal areas were SNR and 0, respectively. A complex random number was added to each pixel of the image to simulate Gaussian distributed noise having a standard deviation of 1 such that the signal-to-noise ratio of a conventional image of the object is SNR.

The above sequence, adequate to produce a data file for phase image display, was repeated two more times with $2\pi\gamma F_0 t_0^2 = 0$ and -0.6 rad/cm/s to produce a data file for flow-enhanced image display via the weighted sum of Eq. (6). Image pixel intensity was defined as φ for phase display and A for flow-enhanced display, where $A\exp(i\varphi)$ represents each complex pixel value of their associated data files.

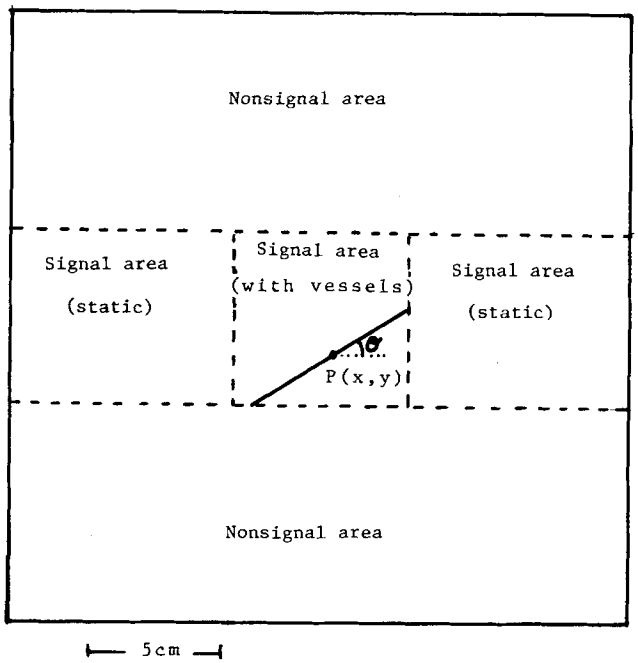

FIG. 1. Simulated object: central area contains N vessels whose locations (x, y coordinates of point P) and directions of flow θ, are selected by a random number generator.

RESULTS

Figures 2–5 are 117×117, 2-mm pixel, phase and flow-

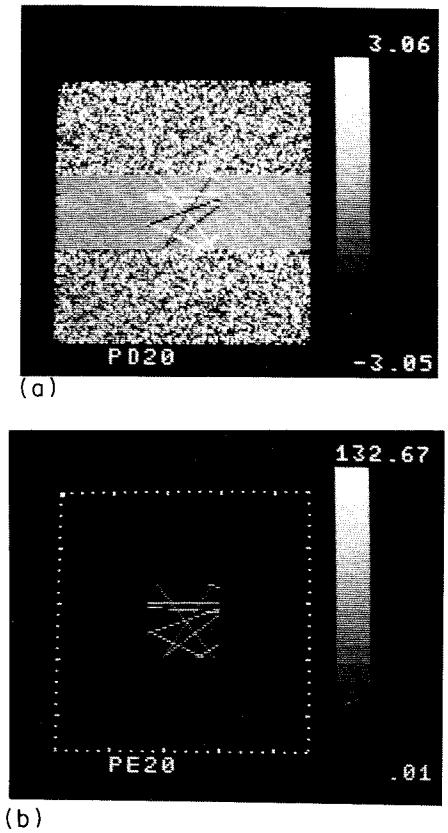

FIG. 2. Simulated (a) phase image and (b) flow-enhanced image where SNR = 30, number of vessels $N = 10$, vessel width $w = 2$ mm, and flow speed $v = 5$ cm/s.

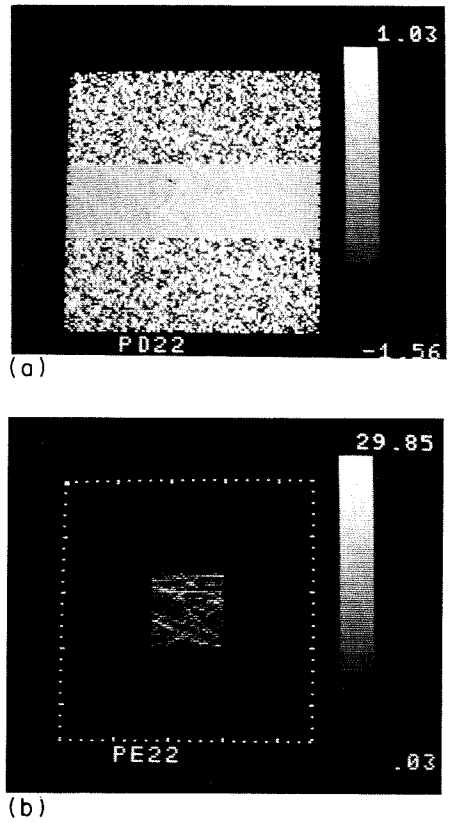

FIG. 4. Simulated (a) phase image and (b) flow-enhanced image where SNR = 30, $N = 50$, $w = 0.2$ mm, and $v = 5$ cm/s.

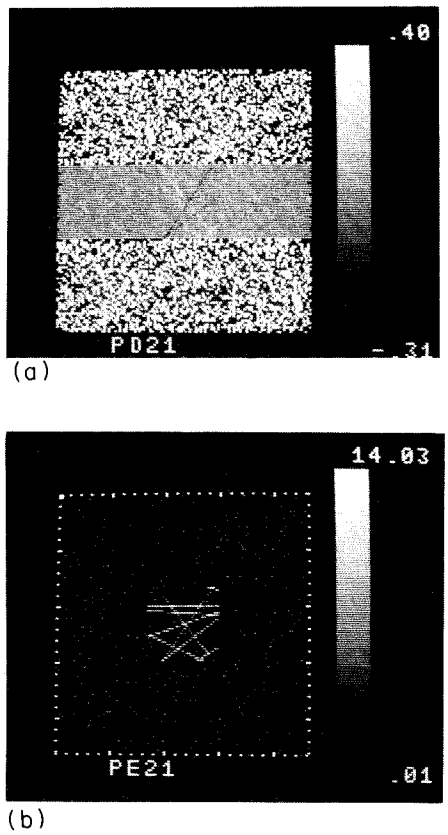

FIG. 3. Simulated (a) phase image and (b) flow-enhanced image where SNR = 30, $N = 10$, $w = 0.2$ mm, and $v = 5$ cm/s.

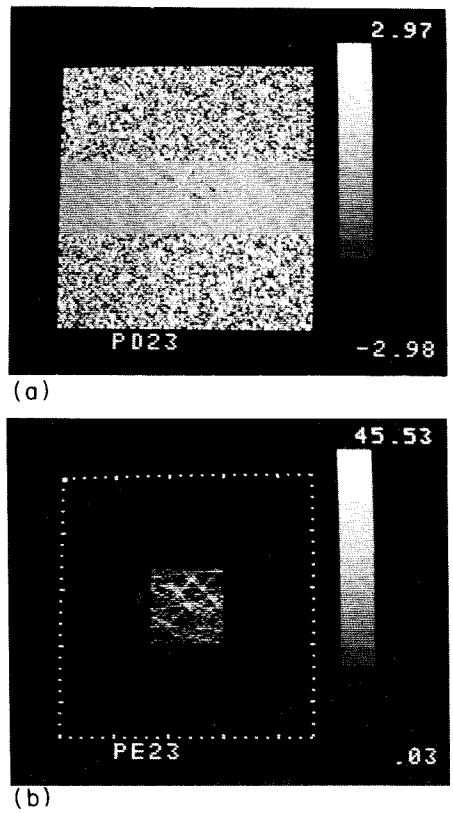

FIG. 5. Simulated (a) phase image and (b) flow-enhanced image where SNR = 30, $N = 100$, $w = 0.2$ mm, and $v = 5$ cm/s.

enhanced images of the object illustrated in Fig. 1. Gray scales of the phase images are windowed to the maximum and minimum of the flow region to optimize contrast of this area. The signal amplitude SNR was set to 30 and flow speed $v = 5$ cm/s was optimal for the prescribed flow gradient.

In Figs. 2(a) and 2(b) are the phase image and flow-enhanced images, respectively, where $N = 10$ vessels having width $w = 2$ mm were prescribed. Notice that, as anticipated, the more the vessel's flow direction is in line with the direction of the applied flow gradient (horizontal), the greater the contrast of the vessel. While the phase image displays directionality of flow as brighter or darker relative to the midgray static tissue, the flow-enhanced method rectifies effects of flow, and suppresses nonsignal and static tissue areas equally. Decreasing the size of the vessels to $w = 0.2$ mm and increasing the number of vessels from $N = 10$ (Fig. 3) to $N = 50$ (Fig. 4) and $N = 100$ (Fig. 5), we see that detectability of the flow region remains relatively low in the phase images. In fact, if the gray scale is windowed to the full $\pm \pi$ range, flow would not be observed at all in Figs. 3(a) and 4(a). On the other hand, the flow-enhanced detectability increases with the number of vessels. While the volumes of flow prescribed in Figs. 2 and 5 are roughly equal, flow conspicuity of the phase image in Fig. 5 is greatly diminished because of phase cancellation effects of many vessels having flow in arbitrary directions. In contrast, the flow-enhanced method adds all flow synergistically, regardless of in-plane directionality.

CONCLUSION

A new method for dectection of flow is introduced and compared to an existing flow imaging technique via computer simulation. The simulation study demonstrates the potential value of the described flow-enhanced imaging technique in detection of highly vascularized areas containing many small entangled vessels in which there is no predominant flow direction. In such cases, the lack of coherence of the contributors of flow phase shifts reduces a phase display to a noiselike appearance, whereas the flow-enhanced results are resistant to random flow direction loss. Furthermore, the flow-enhanced display is derived from the modulus of a reconstructed data set, thereby removing systematic phase errors which may dominate phase images if left uncorrected.

The flow-enhanced technique was designed originally for detection of vascular breast tumors, since the breast may be immobilized relatively easily with patient prone and breast suspended; however, such an approach may also be particularly useful in sensing similar lesions in the extremities, head, and other regions where the imaged volume is relatively stationary.

Until realistic complications such as pulsatility of flow and bulk motion of the imaged object are incorporated into simulations, or until these methods are compared experimentally, it will be difficult to ascertain their limits of flow detectability. Nevertheless, since both phase display and flow-enhanced simulations took advantage of the same ideal conditions in this simulation study, it is anticipated that the flow-enhanced method would yield superior results in instances of complicated vascularity patterns, such as those encountered in the breast tumors.

ACKNOWLEDGMENT

This work was supported in part by PHS Grant No. R01 CA 31857 from the National Cancer Institute, DHHS.

[1]J. R. Singer, in *Nuclear Magnetic Resonance Imaging*, edited by C. L. Partain, A. E. James, Jr., F. D. Rollo, and R. R. Price (Saunders, Philadelphia, 1983), pp. 168–178.
[2]D. A. Feinberg, L. Crooks, J. Hoenninger III, M. Arakawa, and J. Watts, Radiology **153**, 177 (1984).
[3]J. R. Singer, L. E. Crooks, D. Feinberg, and B. Barker, in Proceedings of the Third Annual Meeting of the Society of Magnetic Resonance Imaging in Medicine, Berkeley, CA, 1983, p. 684.
[4]F. W. Wehrli, A. Shimakawa, J. MacFall, and W. Perman, in Proceedings of the Third Annual Meeting of the Society of Magnetic Resonance Imaging in Medicine, Berkeley, CA, 1983, p. 744.
[5]V. Waluch and W. G. Bradley, J. Comput. Assist. Tomogr. **8**, 594 (1984).
[6]M. O'Donnell, Med. Phys. **12**, 59 (1985).
[7]D. J. Bryant, J. A. Payne, D. N. Firmin, and D. B. Tangmore, J. Comput. Assist. Tomogr. **8**, 588 (1984).
[8]V. J. Wedeen, B. R. Rosen, D. Chesler, and T. J. Brady, in Proceedings of the Third Annual Meeting of the Society of Magnetic Resonance Imaging in Medicine, Berkeley, CA, 1983, p. 742.
[9]P. Van Dijk, J. Comput. Assist. Tomogr. **8**, 429 (1984).
[10]P. R. Moran, Magn. Reson. Imag. **1**, 197 (1982).
[11]P. R. Moran, R. A. Moran, and N. Karstaedt, Radiology **154**, 433 (1985).
[12]D. G. Norris, in Proceedings of the Third Annual Meeting of the Society of Magnetic Resonance Imaging in Medicine, Berkeley, CA, 1983, p. 559.
[13]P. N. Burns, M. Halliwell, and P. N. T. Wells, Ultrasound Med. Biol. **8**, 127 (1982).